applied sciences

MDPI

Article

Steel Corrosion Behavior in Light Weight Fly-Ash Based Alkali Activated Mortars

Giulia Masi

Department of Civil, Chemical, Environmental and Materials Engineering, University of Bologna, via Terracini 28, 40131 Bologna, Italy; giulia.masi5@unibo.it; Tel.: +39-0512090361

Abstract: Alkali activated materials as possible sustainable alternative to cementitious binders showed competitive performances in terms of mechanical and durability properties and high temperature stability. For this reason, light weight fly-ash based mortars have already been optimized as passive fire protective coating for steel structures. However, a lack of information about the durability of these innovative systems in terms of steel corrosion resistance is still present. Thus, this study aims at investigating the durability of steel coated with a 20-mm thick light weight mortar layer in a neutral environment (tap water) and in presence of chloride-containing solution (0.2 M NaCl). In addition, the influence of pore solution chemistry and pH was discussed through electrochemical testing in leachate pore solution and NaOH aqueous solutions at different concentrations. It was found that almost complete protection ability of light weight mortar was obtained when coated steel is exposed to neutral solution for 60 days, while in presence of chlorides, steel is more susceptible to corrosion already after 40 days of exposure. In addition, the developed open porosity of the light weight mortars, it was found that pH and the chemistry of the pore solution in contact with steel strongly influenced the steel corrosion resistance.

Keywords: alkali activated materials; steel corrosion; light weight mortars; electrochemical testing; durability; chlorides; coating

Citation: Masi, G. Steel Corrosion Behavior in Light Weight Fly-Ash Based Alkali Activated Mortars. *Appl. Sci.* **2021**, *11*, 1908. https://doi.org/10.3390/app11041908

Academic Editor: Fortunato Crea

Received: 15 January 2021
Accepted: 18 February 2021
Published: 22 February 2021

1. Introduction

Alkali activated materials (AAMs) are one of the possible routes for producing more sustainable construction materials compared to ordinary Portland Cement (OPC), especially when aluminosilicate precursors and/or activators with low environmental impact (i.e., industrial byproducts) are used [1–3]. In general, tailoring the mix designs allows to produce AAMs with high mechanical performances [2,4], good durability [5–8] and outstanding resistance to high temperature [9–11].

In recent years, many research efforts were spent in investigating the corrosion mechanism of steel reinforcements in alkali activated concretes and mortars, due to the carbonation that induces pH lowering [12–14] or due to the presence of aggressive species, especially chloride ions [15–17]. Compared to OPC-based materials, parameters, such as precursor and activator chemistry and concentration, rather than pore distribution, microstructure and composition of the pore solution, can strongly influence the steel corrosion behavior [18]. When low-calcium fly ashes are applied, a strongly alkaline and weakly oxidative environment is provided by pore solution and the passivation mechanism is similar to the one observed in cementitious materials [18–20]. Scattered results have been obtained among different studies that introduced chlorides in the material during mixing or through exposure to chloride-containing solutions [15,16,21–23]. This confirms that factors related to the binder microstructure and to the precursor chemistry, regulate the corrosion behavior. To better investigate these behaviors, electrochemical corrosion tests performed in simulated pore solutions highlighted that the alkalinity strongly influences the

chloride-induced corrosion of the embedded steel [17]. So, due to the fact that low-calcium AAM binders do not contain $Ca(OH)_2$ species performing as pH buffer, as in OPC, long-term durability of steel embedded in low-Ca AAMs is ensured only if the binder is able to retain the alkalinity of the pore solution in contact with steel [18,19].

Furthermore, AAMs have been positively considered when foams and light weight aggregates are applied for high temperature applications. This is related to the fact that light weight AAMs can exhibit low density and thermal conductivity values [9,24], as well as great thermal stability [25–28]. In addition, compared to cement-based materials that are prone to spalling when heated, AAMs (especially low-calcium based-ones) are not subjected to significant damages thanks to different microstructures and to the chemistry of water contained in the matrix. During high temperature exposure, the rapid dehydration of weakly bound water allows the retention of residual mechanical strength and dimensional stability [11]. Recently, light weight AAMs have been specifically applied as fire protection for steel structures producing passive fire protection showing encouraging results [29–32]. In previous studies [24,26,33], the development of light weight mortars based on the alkali activation of low-calcium fly ashes was achieved as passive fire protection. The use of expanded perlite as light aggregates and hydrogen peroxide as foaming agent allowed the preparation of mortars with performances comparable to commercial cement based-passive fire protective coatings [24]. In addition, protection against cellulosic fire was obtained when a 20-mm thick light weight mortar coating was applied on steel, demonstrating the promising performances of these materials as passive fire protection [26,33]. In addition to the measured fire protection, these innovative coatings should also exhibit durability properties, especially in terms of prevention and/or mitigation of steel corrosion phenomena.

For this reason, the present study aims at the assessment of the chloride-induced steel corrosion when light weight alkali activated mortars (LWM) were applied. For comparison seek, normal weight fly ash-based mortars (M) with silica sand as aggregate were also tested in the same conditions to highlight the effect of the mortar porosity related to the presence of the aggressive agents (i.e., chlorides) in the steel corrosion behavior. In a previous study, it was found that the effect of the increased and more interconnected porosity of LWM increased the tendency of the steel corrosion after few days of exposure in 0.6 M sodium chloride aqueous solution (simulating the salt concentration in seawater) [33]. These findings demonstrated that LWM layer is not able to provide suitable protection to steel structures in this harsh environment. However, fireproof coatings can also be applied on steel structures not located in coastal regions, in which the presence of chloride ions is limited to smaller concentrations and/or to seldom events (e.g., distribution of deicing salts in winter season). Therefore, in this study we discussed the durability of the coated steel by immersion in less aggressive environments, i.e., tap water and 0.2 M NaCl aqueous solution, to highlight the durability of the coated systems. Results about the pore size distribution and the microstructure of the two mortars have been also reported to correlate the physical and the durability properties of the developed mortars. Lastly, to investigate the effect of the alkali activated binder on the steel corrosion mechanism, electrochemical testing was carried out in different electrolytes simulating the alkaline environment of the pore solutions (i.e., leachate pore solution and sodium hydroxide (NaOH) aqueous solutions at different pH) with the presence of chlorides.

2. Materials and Methods

2.1. Materials

In this study, EFA-Fuller® low-calcium fly ashes (Class F according to ASTM C618 standard) sourced by BauMineral (Herten, Germany) were applied as precursor. Their chemical composition, measured by inductively coupled plasma optical emission spectroscopy (ICP-OES) is reported as oxides (in wt%), as follows: 58.6 SiO_2, 23.0 Al_2O_3, 0.9 TiO_2, 6.1 Fe_2O_3, 5.9 CaO, 1.8 MgO, 1.1 K_2O, 0.9 Na_2O, 0.9 SO_3, with a loss of ignition of 2.7

wt%. To perform alkali activation, sodium silicate and an 8M sodium hydroxide (ACS reagent NaOH pellets (97%, sourced by Sigma Aldrich, Milan, Italy) aqueous solution were used as activators. The sodium silicate solution (Reoflux B) was supplied by Ingessil S.r.l (Verona, Italy) and it is characterized by the following chemical composition: 29.86% SiO_2, 14.43% Na_2O, 55.71% H_2O, with SiO_2/Na_2O ratio equal to 2.07. To prepare the alkali activated mortars, a normalized silica sand (complied with the EN 196-1 standard) or expanded perlite, both with a fixed grain size distribution (d_{max} = 2 mm), were used as fine aggregates. In addition, a 30 vol% hydrogen peroxide solution (ACS reagent H_2O_2 solution sourced by Sigma Aldrich, Milan, Italy) was applied as a foaming agent for the preparation of light weight mortar samples.

Steel plate (1 mm-thick) specimens applied in this study showed the following chemical composition (in wt%), measured by Glow Discharge Optical Emission Spectroscopy (GDOES, Spectruma Analitik GDA 650, Milan, Italy): 0.04 C, 0.22 Mn, 99.66 Fe with S, P, Cr and Ni in traces. The steel surface was sand blasted before sample preparation, producing a controlled surface finishing characterized by the following roughness parameters: R_a (arithmetic mean deviation of the roughness profile) equal to 4.3 ± 0.6 μm and R_q (root-mean-square deviation of the roughness profile) equal to 5.6 ± 0.7 μm.

2.2. Sample Preparation

Mortars were prepared by mixing fly ash with alkaline solutions, aggregates (silica sand or expanded perlite) and water for 5 min. The detailed procedure for sample preparation is reported in [24,26]. Standard weight (named M) and light weight (named LWM) mortar samples were prepared using silica sand and expanded perlite as aggregates, respectively. In addition, when LWM samples were prepared, a 0.3 wt% of 30 vol% hydrogen peroxide solution was added to the slurry during the last minute of the mix as foaming agent [34]. Table 1 reports the composition of the investigated mortars. The obtained alkali activated mortars exhibited a targeted molar Si/Al ratio of 2.9 and a total water content (considering the amount of water in the activating solutions and the extra water) of 10% and 22% for M and LWM samples, respectively.

Table 1. Mix design of the prepared mortar samples.

Samples	Fly Ash (wt%)	8M NaOH (wt%)	Sodium Silicate (wt%)	Extra Water (wt%)	Silica Sand (wt%)	Expanded Perlite (wt%)	H_2O_2 (wt%)
M	28.3	2.1	10.7	2.2	56.5	-	-
LWM	54.5	4.1	20.5	7.7	-	13.0	0.3

Specimens for physical and microstructural characterization were obtained by pouring the fresh mortars into cylindrical molds (with a diameter of 35 mm). Samples simulating the coated steel structures were prepared by pouring the fresh mortars on the steel plate samples (50 mm × 50 mm × 1 mm) to produce 20 mm-thick coating, as sketched in Figure 1. All the samples were cured in sealed conditions at ambient temperature (T = 21 ± 2 °C) and after 3 days samples were demolded and stored for a total curing time of 28 days.

2.3. Characterization

The mortar characterization was carried out after 28 days of mortar curing. Total open porosity and pore size distribution of the M and LWM mortars were measured by Mercury Intrusion Porosimetry (MIP) using Pascal 140 and 240 instruments (Thermo Fisher Scientific, Como, Italy). MIP analyses were performed on mortar specimens of ~1 cm^3, avoiding the external surfaces of the samples. The microstructure of the obtained mortars was observed by Scanning Electron Microscopy (SEM, Philips XL20, Milan, Italy) using the secondary electron (SE) detector at 10 keV. Prior to SEM observation, samples were sputtered with gold to make them conductive.

Steel plates cover by 20-mm thick coatings made of M and LWM were partially exposed to tap water and in a 0.2 M NaCl aqueous solution for 60 days to test the steel corrosion behavior. Prior to exposure, a Cu-wire was soldered on the steel surface to ensure the electrical conductivity of the steel for electrochemical testing. Then all the sample surfaces, except the top one, were coated with epoxy resin in order to ensure solution penetration by capillary, as detailed in Figure 1.

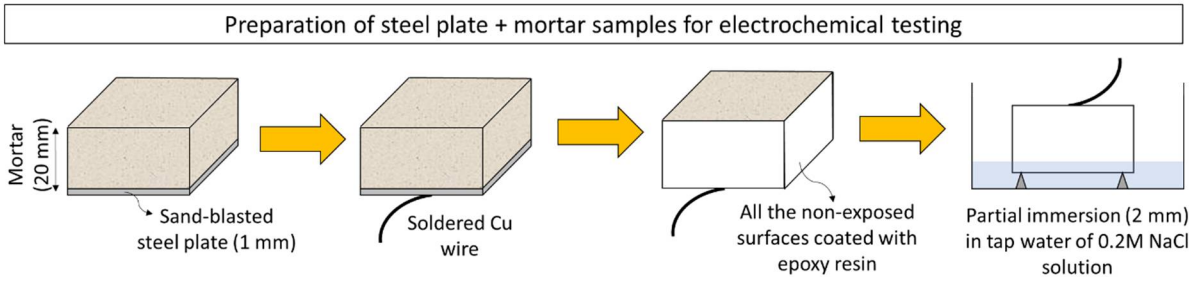

Figure 1. Schematization of the laboratory samples simulating the coated steel structure by 20-mm thick alkali activated mortar (normal weight fly ash-based mortars (M) and light weight alkali activated mortars (LWM)) layers. These samples were used for electrochemical testing.

Samples were partially immersed in 2-mm depth solution in the laboratory conditions. Boxes containing the testing samples were covered to avoid evaporation and solutions were renewed every 14 days. During the exposure, measurements of the corrosion potential (E_{cor}) were daily carried out, as well as anodic polarization curves were recorded after 1 day and at the end of the exposure (after 60 days). Electrochemical tests were performed using an Amel Electrochemistry Potentiostat (model 7050, Milan, Italy), applying the conventional three-electrode cell depicted in Figure 2a: coated steel samples with mortar (M or LWM) layer were set as the working electrode (WE), a saturated calomel electrode (SCE) worked as the reference electrode (RE) and an external stainless steel (SS) net was used as the counter electrode (CE). Polarization curves were carried out after 1 h of immersion in the electrolyte, recording between 0.1 V lower than the open circuit potential (E_{OCP}) up to 1.0 V higher than the E_{OCP}, applying a scan rate of 0.167 mVs^{-1}. At least three samples were tested for all the electrochemical measurements to ensure reproducibility of the results. At the end of exposure low magnification imaging was performed on the steel plate by stereomicroscopy (Olympus SZX10, Milan, Italy).

To investigate the effect of the alkali activated binder on the corrosion behavior of the steel plates, anodic polarization curves of steel samples (named S) were recorded in different environments, using the electrochemical set up previously described. The only differences were (i) the use of a platinum rod as CE and (ii) the application of a Teflon sample holder applied to have a WE with an exposed area of 2.01 cm^2, as shown in Figure 2b. First, leachate pore solution (LPS) was considered as electrolyte for anodic polarization. It was prepared following the procedure reported in [21,35]: alkali activated binder was crushed and mixed with distilled water in 1:1 proportion and stirred for 24 h. Then, this solution was filtered using a vacuum pump and the obtained LPS exhibited a pH of 12.8 and a chemical composition reported in Table 2. The pH of the obtained leachate solution was considered as an acceptable approximation of the pH of the mortar pore solution [21,22].

Table 2. Chemical composition of the leachate pore solution (LPS). The measurements of the most concentrated elements were carried out using a 1:100 diluted solution.

Element	Concentration (mg/L)
Si	2000
Al	6.1
Ti	0.1
Fe	0.6
Ca	4.4
Mg	0.7
K	166
Na	10,300
S	3800

Secondly, anodic polarization curves were recorded in NaOH aqueous solutions with different concentrations (0.1 M and 0.001 M), selected based on the pH of the mortar samples at different curing stages (after 28 days of curing in sealed conditions and after 1 year of exposure at laboratory conditions). pH measurements were carried out mixing 5 g ground mortar samples with 5 cm^3 distilled water, at room temperature. Addition of 0.2 M NaCl was performed in the selected NaOH solutions to simulate the effect of chlorides in steel corrosion.

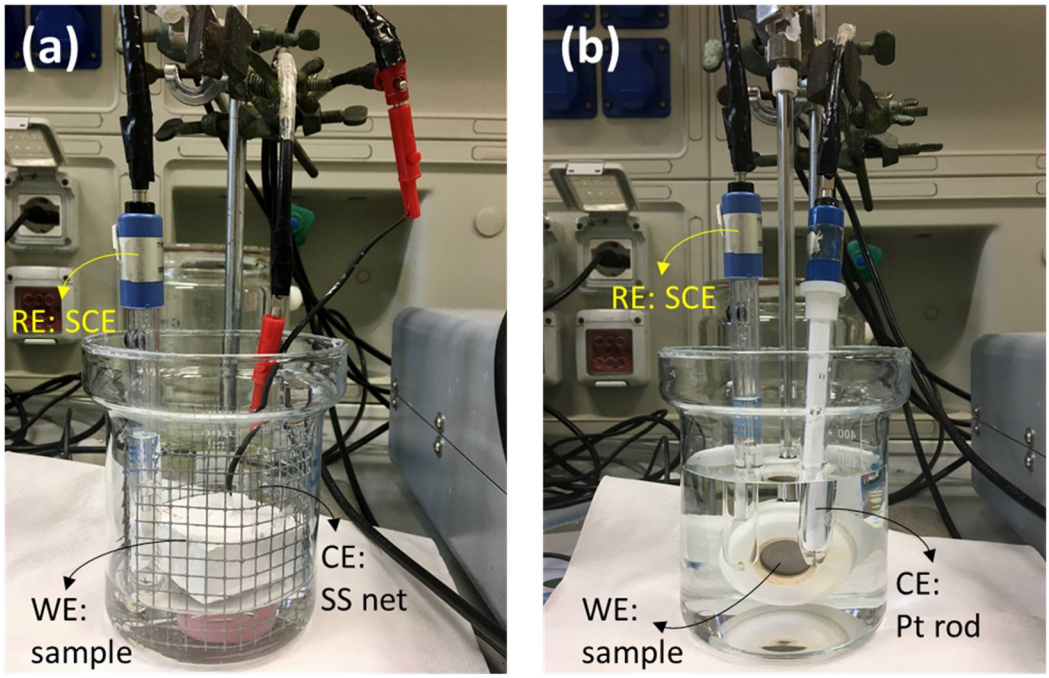

Figure 2. Electrochemical set up consisting of the conventional three-electrode cell for anodic polarization curves of (**a**) coated steel samples with LWM or M mortars and (**b**) steel samples tested in different solutions.

3. Results and Discussion

3.1. Physical Properties and Microstrure

MIP results reported in Figure 3 showed a strong difference in pore size distribution and total open porosity between M and LWM: while M sample exhibited a total cumulative intruded Hg volume of 52 mm^3/g and a total open porosity of 11%, LWM sample showed values of 367 mm^3/g and 48%, respectively. These results confirm the efficiency of H_2O_2 as foaming agent together with the use of expanded perlite as light weight aggregate, as previously observed [24,34]. Furthermore, a strong difference between the two

samples was observed in terms of pore size distribution as reported in Figure 3b. M samples exhibited a bimodal pore distribution mainly in the ranges of 0.020–0.35 μm and 1.50–2.0 μm. Conversely, LWM were characterized by pores in the ranges of 0.020–0.040 μm, 0.080–0.20 μm and bigger pores with dimensions of 1.5–2.0 μm and 3.0–6.0 μm, showing both the contribution of the alkali activated binder and expanded perlite aggregates. The different pore size distributions between M and LWM, depicted in Figure 3, clearly showed that, while small capillary pores are present in M samples (that usually slow down the mortar saturation rate but increase the height of penetration), an increased porosity with also larger pores characterized LWM microstructure. Thus, this induced a faster water absorption but lower penetration height [36]. However, for both the samples, the water penetration surely reached 20 mm that represents the thickness of the mortar coating during the 60-days exposure performed for durability tests.

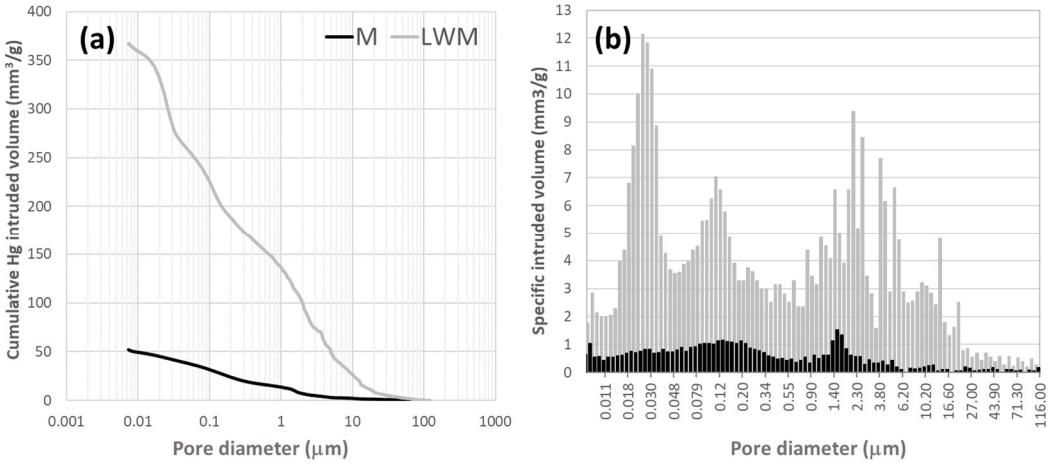

Figure 3. Pore size distribution of LWM and M samples measured by mercury intrusion porosimetry: (**a**) cumulative specific Hg intruded volume versus pore size; (**b**) histograms representing the specific intruded volume in the pore size ranges.

To better characterize the pore distribution and morphology, SEM observation was carried out on fracture surfaces of M and LWM and the results are reported in Figure 4. In particular, Figure 4a,c (at higher magnification) showed the typical microstructure of the fly-ash based alkali activated mortars (M sample): some unreacted fly ashes can be detected within a homogenous and dense gel. Only few pores in the range of 10 to 50 μm were observed at these magnifications. On the contrary, LWM microstructure (reported in Figure 4b,d) showed a more porous matrix, induced by the effect of the foaming agent and the addition of expanded perlite (characterized by a developed open cell porosity). This morphological observation confirms the results on pore size distribution previously discussed.

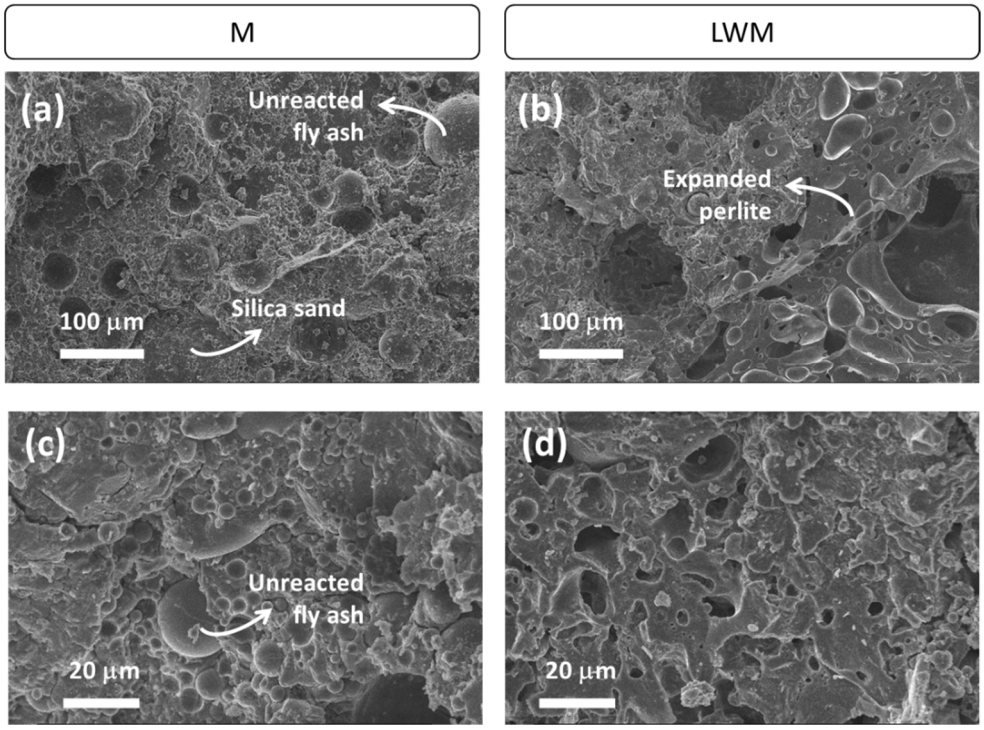

Figure 4. SEM morphological observation of (**a**,**c**) M and (**b**,**d**) LWM samples at different magnifications: (**a**,**b**) at 200 × and (**c**,**d**) at 1000 ×.

3.2. Corrosion Behavior of Coated Steel with Mortars

Evolution of the open circuit potential (E_{cor}) in the M and LWM coated steel samples during exposure in tap water and in 0.2 M NaCl solution for 60 days is reported in Figure 5. Initially, at the beginning of the exposure test, both samples exhibited E_{cor} values in the range between −0.15 V vs. SCE and 0.00V vs. SCE, indicating that steel was in the passive state during mortar curing [18,21]. Different potential behavior was observed considering the two exposure conditions. Firstly, when coated steel samples with LWM layer were exposed to tap water (the less aggressive environment with average chloride concentration of 27 mg/L [37]), E_{cor} values fluctuated between −0.30 V vs. SCE and −0.10 V vs. SCE for the whole exposure (60 days), as shown in Figure 5a. This potential fluctuation could be related to the changing in pH of the solution due to the leaching of the free alkalis present in the mortars [19]. For this reason, to ensure the aggressiveness of the electrolyte, solutions were renewed every 14 days (highlighted in Figure 5 by vertical dot lines). Similar behavior was observed also for E_{cor} values of M samples. In the latter case, a stronger value fluctuation was detected in the first 10 days of exposure, when E_{cor} reached −0.40 V vs. SCE. This is probably related to the different pore size distribution between M and LWM (as highlighted in Figure 3), in the sense that M is mainly characterized by capillary pores that are usually responsible of a higher penetration depth compared to the larger pores present in LWM [36]. In the case of exposure to chloride-containing solution, both samples exhibited almost constant E_{cor} values between −0.20 V vs. SCE and −0.10 V vs. SCE within 40 days of exposure. For longer time, E_{cor} started to decrease for both samples and reached values around −0.50 V vs. SCE at the end of the exposure. In addition, LWM samples showed more scattered results probably indicating a slightly greater tendency to corrosion compared to M.

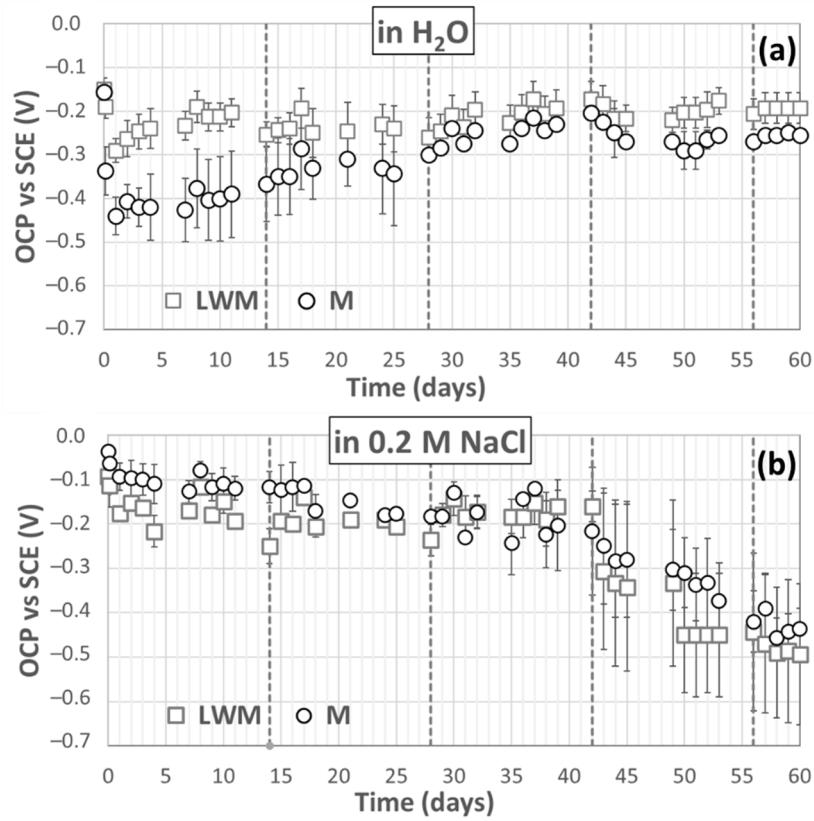

Figure 5. Average corrosion potential values (E_{cor}) for M (square) and LWM (circle) samples during the 60 days partial immersion in (**a**) tap water and (**b**) 0.2 M NaCl aqueous solutions. Vertical dot lines represent solution renewal every 14 days.

At the end of the exposure in both the solutions, the mortar layers were removed by the steel plates to observe the steel surface and the possible corrosion products precipitated at the steel-mortar interface. Results are reported in Figure 6.

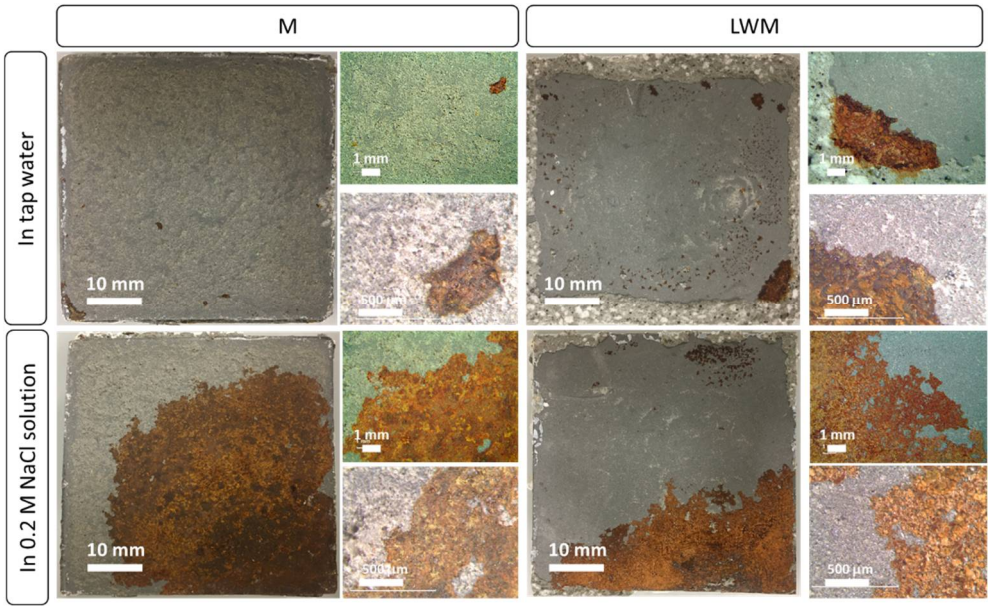

Figure 6. Macro and low magnification images of the carbon steel plates coated with 20 mm thick M or LWM layers after 60 days of immersion in tap water and in 0.2 M NaCl aqueous solution.

On steel samples exposed in tap water, the extent of corrosion products was limited to few surface areas, especially when M was applied as coating. In this sample, only four surface portions, in which corrosion products have been precipitated, were detected. For LWM coated steel samples exposed in water, localized precipitation of corrosion products was observed along the steel surface together with a more extended area of corrosion products close to a sample edge.

Conversely, different features were observed for steel samples exposed to chloride-containing solution. Both steel plates covered with LWM and M exhibited a more pronounced corroded surface (i.e., rust) distributed on the steel specimen, compared to tap water exposure. In particular, both samples exhibited the precipitation of rust close to a sample edge, indicating that the peripheral parts of the coated samples are more susceptible to defects that are induced by steel cutting and/or mortar preparation. Moreover, a larger extent of corroded surface was detected in M sample compared to LWM, indicating that, even if E_{cor} values showed a similar trend (depicted in Figure 5b), the corrosion process was characterized by a faster corrosion rate for M sample. This could be related to the presence of a larger number of capillary pores that allowed the aggressive solution to firstly reached the steel surface than LWM sample [36]. At last, the morphological observations reported in Figure 6 are in accordance with the recorded E_{cor}, confirming that the corrosion potential decrease after 40 days of exposure in chloride-containing solution corresponded to steel corrosion condition.

Figure 7 reports the anodic polarization curves obtained from M and LWM coated steel samples exposed in tap water and 0.2 M NaCl chloride solution. For each exposure, anodic polarization curves were recorded after 1 day and 60 days (end of exposure) of partial immersion. For short exposure (1 day), all the anodic polarization curves showed a value of E_{OCP} of −0.2 V vs. SCE and a passive behavior with low values of corrosion current densities (i_{cor}). For M sample, an order of magnitude was recorded between i_{cor} values measured in the two different solutions: $1.5 \cdot 10^{-9}$ A/cm^2 in tap water and $1.7 \cdot 10^{-8}$ A/cm^2 in chloride-containing solution. However, LWM exhibited comparable i_{cor} results of $5.0 \cdot 10^{-8}$ A/cm^2 for both the tested environments. After 60 days of exposure, all the anodic polarization curves showed more electronegative E_{OCP} values. In particular, E_{OCP} of −0.4 V vs. SCE and −0.6 V vs. SCE were measured for samples exposed in tap water and chloride-containing solution, respectively. These values well corresponded to the corrosion potentials reported in Figure 5 after 60 days of exposure. In addition, an increase in i_{cor} values was detected especially for LWM sample exposed in chloride-containing solution that exhibited the greatest corrosion current density of $2.7 \cdot 10^{-7}$ A/cm^2. This could be related to the fact that the larger extent of corrosion products, precipitated on steel surfaces when M layer was applied, acted as a physical barrier, slowing down the corrosion kinetic measured by anodic polarization curves for M sample ($i_{cor} = 9.5 \cdot 10^{-8}$ A/cm^2). Thus, chloride-containing solution induced the more relevant changes in polarization curves at the end of exposure, especially for LWM sample.

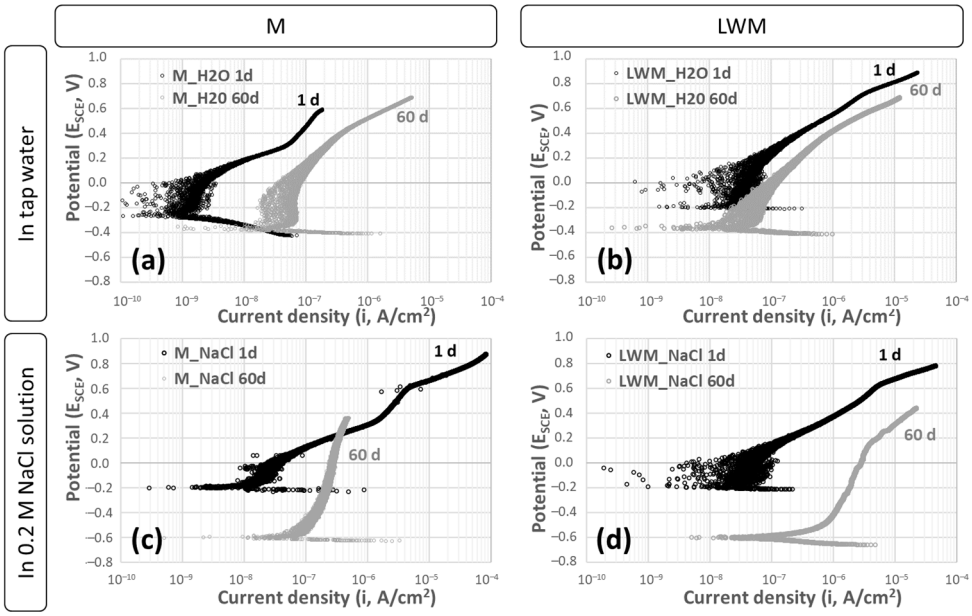

Figure 7. Anodic polarization curves obtained from (**a**,**c**) M and (**b**,**d**) LWM coated steel recorded in in (**a**,**b**) tap water and (**c**,**d**) 0.2 M NaCl aqueous solution. The electrochemical polarization tests were carried out after 1 day (in black) and at the end (60 days) of the partial immersion (in grey) in solutions.

The investigation of corrosion behavior of coated steel with LWM mortars, and its comparison with M mortars, highlighted that the presence of chloride ions fastened the occurring of corrosion. This was demonstrated (i) by the lowering of E_{cor} values to more electronegative potentials after 40 days of exposure, (ii) by the larger extent of corrosion products observed in the steel surfaces and (iii) by the higher i_{cor} values, when compared to tap water exposure. Secondly, it was observed that the different pore size distribution of M and LWM layers partially influence the steel corrosion behavior. This was demonstrated (i) by comparable E_{cor} values between LWM and M in both the tested environments, and (ii) by comparable i_{cor} values recorded after 60 days of exposure by anodic polarization curves, especially for tap water exposure. Lastly, increasing the aggressiveness of the electrolyte (by adding 0.2 M NaCl in aqueous solution) induced a larger extent of corroded surfaces, compared to tap water exposure. All the presented results allowed to conclude that, due the fact that LWM and M mortars were prepared using the same mix design of the binder (precursor and activating solution), also the binder pH and the composition of the pore solution in contact with steel could influence the corrosion behavior of the coated steel, as demonstrated also in other studies [18,21,38].

3.3. Corrosion Behavior of Steel in Solutions

To deeply investigate the parameters related to binder chemistry, Figure 8 collects the anodic polarization curves recorded in the leachate pore solution (LPS, with a pH of 12.8) obtained from the alkali activated binder tested in this study. It clearly shows that in both cases steel exhibited a passive behavior at E_{OCP} close to −0.3 V vs. SCE for leachate solution and −0.5 V vs. SCE when chloride ions (using 0.2 M NaCl) were added. In leachate solution, a passivity range of 0.9 V was observed between −0.3 V vs. SCE and +0.6 V vs. SCE. Similar results were obtained in different fly-ash based leachate solutions [21], indicating that alkali activation of fly ash allowed comparable steel corrosion protection, even if its source, chemistry and composition are different. At the end of the polarization, the visual inspection did not reveal any corroded surface. On the contrary, when chloride ions were added in the leachate pore solution, a smaller and less stable passive region of 0.5–0.6 V was observed between −0.5 V vs. SCE and +0.07 V vs. SCE. Consequently, higher

corrosion current density was also measured: i_{cor} values of $8.8 \cdot 10^{-6}$ A/cm^2 in contact with chlorides and $5.0 \cdot 10^{-7}$ A/cm^2 in leachate pore solution.

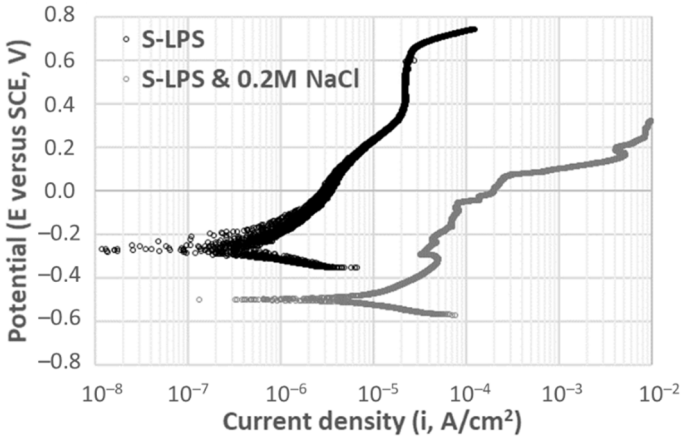

Figure 8. Anodic polarization curves of sand blasted steel (S) in leachate pore solution without (in black) and with 0.2 M NaCl (in grey).

pH measurements of the investigated mortars were carried out as a function of time. After 28 days of curing, they exhibited a pH of 12.8. This high alkalinity is maintained if samples are stored in sealed conditions, while samples exposed to laboratory showed a decrease in pH values due to carbonation: pH of 11.2 and 10.9 was measured after 56 days and 365 days, respectively. In order to investigate the effect of decreasing pH of the pore solution in steel corrosion behavior, anodic polarization curves were recorded in NaOH aqueous solution with pH comparable to the ones measured in the real mortars. For this reason, NaOH concentrations of 0.1 M and 0.001 M were selected to reproduce the alkalinity of the pore solution at the end of the mortar curing period (pH ~ 13) and after one-year exposure at atmosphere (pH ~ 11). Results, reported in Figure 9a, showed similar shapes of the polarization curves recorded in 0.1 M NaOH solution compared to the ones in LPS. This is mainly because both the electrolytes had the same pH. However, different i_{cor} values were obtained: higher current densities of $2.6 \cdot 10^{-6}$ A/cm^2 (without chloride ions) and $2.3 \cdot 10^{-5}$ A/cm^2 (with chloride ions) were measured in 0.1 M NaOH solution. This result indicates that the presence of other elements in the leachate pore solution (e.g., silicates) could act as corrosion inhibitor and enhanced the steel corrosion resistance [21]. Lastly, lowering the pH down to 10.9 (by 0.001 M NaOH solution) induced a strong change in both the polarization curves (Figure 9b): the passive region disappeared meaning that this environment is not able to passivate the steel. However, similar i_{cor} values were recorded for this NaOH concentration of about $3.0 \cdot 10^{-6}$ A/cm^2 (without chloride ions) and $3.2 \cdot 10^{-5}$ A/cm^2 (with chloride ions). These results highlight the necessity to have a highly alkaline environment close to steel–mortar interface to maintain steel in the passive state. To avoid lowering of the pore solution pH, a possible solution could be the application of a post-treatment (e.g., sealing) on the LWM layer, that could mitigate the carbonation of the alkali activated binder exposed to atmosphere, and slow down the ingress of aggressive species, as chloride ions. A particular attention should be paid on the choice of the kind of treatment since it should exhibit passive fire protection properties as well as the 20-mm thick LWM layer.

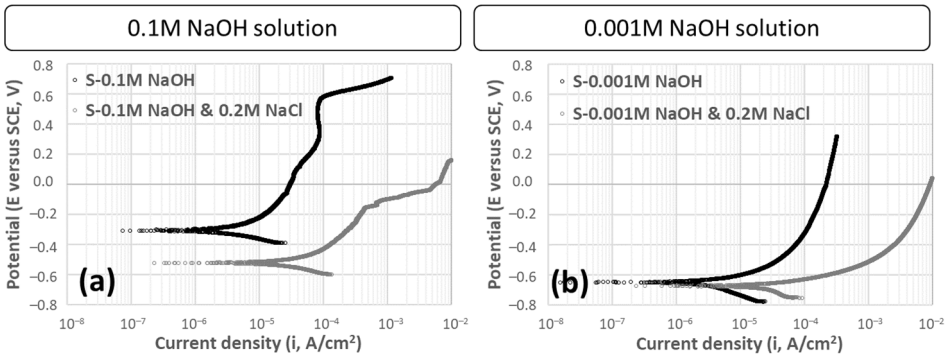

Figure 9. Anodic polarization curves of sand blasted steel (S) in (**a**) 0.1 M NaOH and (**b**) 0.001 M NaOH aqueous solutions without and with the addition of 0.2 M NaCl.

4. Conclusions

Durability results were first achieved in this study in terms of chloride-induced corrosion of steel coated with light weight alkali activated mortars optimized for fire protection applications by electrochemical techniques.

Exposure to neutral environment (tap water) showed encouraging results since similar behavior in corrosion potential and anodic polarization curves was observed regardless the different pore distribution of the mortar layers. For the 60-day exposure in tap water, similar corrosion potentials and corrosion current density values were obtained by both light and normal weight mortars. However, an increase of aggressiveness of the electrolyte (0.2 M NaCl aqueous solution) induced that after 40 days of exposure, steel started to corrode, as depicted by corrosion potential values. Compared to steel samples covered by light weight mortar, normal weight mortar layer exhibited a larger extent of corrosion products precipitated on steel surfaces at the end of exposure, which acted as physical barrier producing a slowdown in the corrosion current density values measured by anodic polarization curves.

Results of the electrochemical investigation of steel coated with light and normal weight mortars suggested that other aspects are also influencing the corrosion mechanisms, due to the fact that same mix design was applied for both the mortar layer. Indeed, it was found that the environment of the pore solution (pH and composition) in the binder strongly influenced the steel corrosion behavior. Leachate pore solution obtained from the 28-days cured mortars (pH = 12.8) allowed passivation of the steel, as highlighted by anodic polarization curves. However, the lowering of mortar pH (pH ~ 11) measured after one-year exposure to the atmosphere did not allow steel passivation, thus steel corrosion protection is not completely guaranteed. Further analyses of the morphology and composition of corrosion products formed in the different tested solutions are planned to confirm this point. In addition, the effect of chloride addition increased the corrosion current densities values regardless of the solution pH and in the case of leachate pore solution chlorides are responsible of a less stable and smaller passive region.

Finally, passive fire protective coating consisting in light weight alkali activated mortar can partially ensure durability of the steel structures in terms of steel corrosion mitigation. However, additional solutions should be considered to improve these durability aspects, such as the application of a sealing treatment to applied on the light weight mortar layer, in order to slow down the ingress of aggressive species, i.e., chloride ions, and carbonation phenomena.

Funding: This research received no external funding.

Institutional Review Board Statement: Not applicable.

Informed Consent Statement: Not applicable.

Data Availability Statement: The data presented in this study are available on request from the corresponding author. The data are not publicly available due to confidentiality reason.

Acknowledgments: Iuri Boromei, Alessandro Filipponi, and Enrico Sassoni are acknowledged for their valuable help in characterization techniques. The author would thank Maria Chiara Bignozzi for valuable discussion and Chiara Santori for the help in the experimental.

Conflicts of Interest: The authors declare no conflict of interest.

References

1. Provis, J.L. Alkali-activated materials. *Cem. Concr. Res.* **2018**, *114*, 40–48, doi:10.1016/j.cemconres.2017.02.009.
2. Shi, C.; Qu, B.; Provis, J.L. Recent progress in low-carbon binders. *Cem. Concr. Res.* **2019**, *122*, 227–250, doi:10.1016/j.cemconres.2019.05.009.
3. Wu, Y.; Lu, B.; Bai, T.; Wang, H.; Du, F.; Zhang, Y.; Cai, L.; Jiang, C.; Wang, W. Geopolymer, green alkali activated cementitious material: Synthesis, applications and challenges. *Constr. Build. Mater.* **2019**, *224*, 930–949, doi:10.1016/j.conbuildmat.2019.07.112.
4. Ding, Y.; Dai, J.G.; Shi, C.J. Mechanical properties of alkali-activated concrete: A state-of-the-art review. *Constr. Build. Mater.* **2016**, *127*, 68–79, doi:10.1016/j.conbuildmat.2016.09.121.
5. Mundra, S.; Bernal, S.; Provis, J. Corrosion initiation of steel reinforcement in simulated alkali-activated slag pore solution. In Proceedings of the 1st International Conference on Construction Materials for Sustainable Future, Zadar, Croatia, 19-21 April 2017.
6. Provis, J.L.; Bernal, S.A. Geopolymers and Related Alkali-Activated Materials. *Annu. Rev. Mater. Res.* **2014**, *44*, 299–327, doi:10.1146/annurev-matsci-070813-113515.
7. Bernal, S.A.; Provis, J.L. Durability of alkali-activated materials: Progress and perspectives. *J. Am. Ceram. Soc.* **2014**, *97*, 997–1008, doi:10.1111/jace.12831.
8. Winnefeld, F.; Gluth, G.; Bernal, S.; Bignozzi, M.; Carabba, L.; Chithiraputhiran, S.; Dehghan, A.; Dolenec, S.; Dombrowski-Daube, K.; Dubey, A.; et al. RILEM TC 247-DTA round robin test: Sulfate resistance, alkali-silica reaction and freeze–thaw resistance of alkali-activated concretes. *Mater. Struct. Constr.* **2020**, *53*, 1–17, doi:10.1617/s11527-020-01562-0.
9. Novais, R.M.; Pullar, R.C.; Labrincha, J.A. Geopolymer foams: An overview of recent advancements. *Prog. Mater. Sci.* **2020**, *109*, 100621, doi:10.1016/j.pmatsci.2019.100621.
10. Yang, X.; Chen, S.Y.; Cotton, J.D.; Zhang, Y. Phase stability of low-density, multiprincipal component alloys containing aluminum, magnesium, and lithium. *Jom* **2014**, *66*, 2009–2020.
11. Fan, F.; Liu, Z.; Xu, G.; Peng, H.; Cai, C.S. Mechanical and thermal properties of fly ash based geopolymers. *Constr. Build. Mater.* **2018**, *160*, 66–81, doi:10.1016/j.conbuildmat.2017.11.023.
12. Cyr, M.; Pouhet, R. Carbonation in the pore solution of metakaolin-based geopolymer. *Cem. Concr. Res.* **2016**, *88*, 227–235, doi:10.1016/j.cemconres.2016.05.008.
13. Bernal, S.; San Nicolas, R.; Provis, J.; Mejía De Gutiérrez, R.; Van Deventer, J. Natural carbonation of aged alkali-activated slag concretes. *Mater. Struct. Constr.* **2014**, *47*, 693–707, doi:10.1617/s11527-013-0089-2.
14. Sufian Badar, M.; Kupwade-Patil, K.; Bernal, S.A.; Provis, J.L.; Allouche, E.N. Corrosion of steel bars induced by accelerated carbonation in low and high calcium fly ash geopolymer concretes. *Constr. Build. Mater.* **2014**, *61*, 79–89, doi:10.1016/j.conbuildmat.2014.03.015.
15. Miranda, J.; Fernández-Jiménez, A.; González, J.; Palomo, A. Corrosion resistance in activated fly ash mortars. *Cem. Concr. Res.* **2005**, *35*, 1210–1217, doi:10.1016/J.CEMCONRES.2004.07.030.
16. Bastidas, D.; Fernández-Jiménez, A.; Palomo, A.; González, J. A study on the passive state stability of steel embedded in activated fly ash mortars. *Corros. Sci.* **2008**, *50*, 1058–1065, doi:10.1016/J.CORSCI.2007.11.016.
17. Mundra, S.; Criado, M.; Bernal, S.; Provis, J. Chloride-induced corrosion of steel rebars in simulated pore solutions of alkali-activated concretes. *Cem. Concr. Res.* **2017**, *100*, 385–397, doi:10.1016/J.CEMCONRES.2017.08.006.
18. Mundra, S.; Bernal Lopez, S.; Criado, M.; Hlaváček, P.; Ebell, G.; Reinemann, S.; Gluth, G.; Provis, J. Steel corrosion in reinforced alkali-activated materials. *RILEM Tech. Lett.* **2017**, *2*, 33–39, doi:10.21809/rilemtechlett.2017.39.
19. Gluth, G.J.G.; Ebell, G.; Hlaváček, P.; Mietz, J. Chloride-induced steel corrosion in alkali-activated fly ash mortar: Increased propensity for corrosion initiation at defects. *Mater. Corros.* **2020**, *71*, 749–758, doi:10.1002/maco.202011541.
20. Tittarelli, F.; Mobili, A.; Giosuè, C.; Belli, A.; Bellezze, T. Corrosion behaviour of bare and galvanized steel in geopolymer and ordinary Portland Cement based mortars with the same strength class exposed to chlorides. *Corros. Sci.* **2018**, *134*, 64–77, doi:10.1016/J.CORSCI.2018.02.014.
21. Monticelli, C.; Natali, M.; Balbo, A.; Chiavari, C.; Zanotto, F.; Manzi, S.; Bignozzi, M. Corrosion behavior of steel in alkali-activated fly ash mortars in the light of their microstructural, mechanical and chemical characterization. *Cem. Concr. Res.* **2016**, *80*, 60–68, doi:10.1016/j.cemconres.2015.11.001.
22. Monticelli, C.; Natali, M.; Balbo, A.; Chiavari, C.; Zanotto, F.; Manzi, S.; Bignozzi, M. A study on the corrosion of reinforcing bars in alkali-activated fly ash mortars under wet and dry exposures to chloride solutions. *Cem. Concr. Res.* **2016**, *87*, 53–63, doi:10.1016/j.cemconres.2016.05.010.

23. Criado, M.; Bastidas, D.; Fajardo, S.; Fernández-Jiménez, A.; Bastidas, J. Corrosion behaviour of a new low-nickel stainless steel embedded in activated fly ash mortars. *Cem. Concr. Compos.* **2011**, *33*, 644–652, doi:10.1016/j.cemconcomp.2011.03.014.
24. Carabba, L.; Moricone, R.; Scarponi, G.E.; Tugnoli, A.; Bignozzi, M. Alkali activated lightweight mortars for passive fire protection: A preliminary study. *Constr. Build. Mater.* **2019**, *195*, 75–84, doi:10.1016/j.conbuildmat.2018.11.005.
25. Masi, G.; Rickard, W.; Bignozzi, M.; Van Riessen, A. The effect of organic and inorganic fibres on the mechanical and thermal properties of aluminate activated geopolymers. *Compos. Part B Eng.* **2015**, *76*, 218–228, doi:10.1016/j.compositesb.2015.02.023.
26. Carabba, L.; Pirskawetz, S.; Krüger, S.; Gluth, G.; Bignozzi, M. Acoustic emission study of heat-induced cracking in fly ash-based alkali-activated pastes and lightweight mortars. *Cem. Concr. Compos.* **2019**, *102*, 145–156, doi:10.1016/j.cemconcomp.2019.04.013.
27. Gluth, G.; Rickard, W.; Werner, S.; Pirskawetz, S. Acoustic emission and microstructural changes in fly ash geopolymer concretes exposed to simulated fire. *Mater. Struct. Constr.* **2016**, *49*, 5243–5254, doi:10.1617/s11527-016-0857-x.
28. Rickard, W.; Vickers, L.; van Riessen, A. Performance of fibre reinforced, low density metakaolin geopolymers under simulated fire conditions. *Appl. Clay Sci.* **2013**, *73*, 71–77, doi:10.1016/j.clay.2012.10.006.
29. Sakkas, K.; Sofianos, A.; Nomikos, P.; Panias, D. Behaviour of Passive Fire Protection K-Geopolymer under Successive Severe Fire Incidents. *Materials* **2015**, *8*, 6096–6104, doi:10.3390/ma8095294.
30. Temuujin, J.; Minjigmaa, A.; Rickard, W.; Van Riessen, A. Thermal properties of spray-coated geopolymer-type compositions. *J. Therm. Anal. Calorim.* **2012**, *107*, 287–292.
31. Temuujin, J.; Minjigmaa, A.; Rickard, W.; Lee, M.; Williams, I.; van Riessen, A. Fly ash based geopolymer thin coatings on metal substrates and its thermal evaluation. *J. Hazard. Mater.* **2010**, *180*, 748–752, doi:10.1016/j.jhazmat.2010.04.121.
32. Watolla, M.B.; Gluth, G.; Sturm, P.; Rickard, W.; Krüger, S.; Schartel, B. Intumescent geopolymer-bound coatings for fire protection of steel. *J. Ceram. Sci. Technol.* **2017**, *8*, 351–364, doi:10.4416/JCST2017-00035.
33. Carabba, L.; Masi, G.; Pirskawetz, S.; Krüger, S.; Gluth, G.; Bignozzi, M. Thermal properties and steel corrosion in light-weight alkali activated mortars. In Proceedings of the International Conference on Sustainable Materials, Systems and Structures (SMSS 2019) New Generation of Construction Materials, Rovinj, Croatia, 20–22 March 2019; pp. 125–132.
34. Masi, G.; Rickard, W.; Vickers, L.; Bignozzi, M.; van Riessen, A. A comparison between different foaming methods for the synthesis of light weight geopolymers. *Ceram. Int.* **2014**, *40*, 13891–13902, doi:10.1016/j.ceramint.2014.05.108.
35. Shi, J.; Ming, J.; Sun, W. Electrochemical performance of reinforcing steel in alkali-activated slag extract in the presence of chlorides. *Corros. Sci.* **2018**, *133*, 288–299, doi:10.1016/j.corsci.2018.01.043.
36. Pia, G.; Sassoni, E.; Franzoni, E.; Sanna, U. Predicting capillary absorption of porous stones by a procedure based on an intermingled fractal units model. *Int. J. Eng. Sci.* **2014**, *82*, 196–204, doi:10.1016/j.ijengsci.2014.05.013.
37. Gruppo Hera: Analytical results of potable water in Bologna city Available online: www.gruppohera.it/gruppo/attivita_servizi/business_acqua/qualita/qualita_acqua_hera/qualita_media_comuni/-bologna/pagina281.html (accessed on 17 December 2020).
38. Gunasekara, C.; Law, D.; Bhuiyan, S.; Setunge, S.; Ward, L. Chloride induced corrosion in different fly ash based geopolymer concretes. *Constr. Build. Mater.* **2019**, *200*, 502–513, doi:10.1016/j.conbuildmat.2018.12.168.